

Heat Dissipation Mechanism at Carbon Nanotube Junctions on Silicon Oxide Substrate

Liang Chen
e-mail: lchen64@gatech.edu

Satish Kumar
e-mail: satish.kumar@me.gatech.edu

G.W. Woodruff School of Mechanical Engineering
Georgia Institute of Technology, Atlanta, Georgia, 30332, USA

ABSTRACT

This study investigates heat dissipation at carbon nanotube (CNT) junctions supported on silicon dioxide substrate using molecular dynamics simulations. The temperature rise in a CNT (~top CNT) not making direct contact with the oxide substrate but only supported by other CNTs (~bottom CNT) is observed to be hundreds of degree higher compared to the CNTs well-contacted with the substrate at similar power densities. The analysis of spectral temperature decay of CNT-oxide system shows very fast intra-tube energy transfer in a CNT from high frequency band to intermediate frequency bands. The low frequency phonon band (0-5 THz) of top CNT shows two-stage energy relaxation which results from the efficient coupling of low frequency phonons in the CNT-oxide system and the blocking of direct transport of high and intermediate frequency phonons of top CNT to the oxide substrate by bottom CNT.

KEYWORDS: carbon nanotube network, molecular dynamics, phonons, interfacial thermal transport

1 INTRODUCTION

Due to the exceptional electronic, thermal, and mechanical properties [1] of carbon nanotubes (CNTs), their networks and arrays have been widely investigated for thin-film transistors (TFTs) [2] on flexible or transparent substrates to improve the performance in diverse applications such as liquid crystal displays, sensors, and flexible antennae and radar [3-5]. The fabrication of fully transparent and mechanically flexible TFTs using aligned CNT arrays or a random network of CNTs have demonstrated

high potential of CNT networks for next generation display technologies [6, 7]. In a transparent or flexible display, the carbon nanotube network based thin film transistors (CN-TFTs) will be placed between glass or polymer which have low thermal conductivity. Besides, their surfaces are usually cooled only through natural convection which can make self-heating critical especially for CN-TFTs operating in high frequency range (\sim MHz) [8, 9]. Although CNTs have high thermal conductivity [10, 11], the interfacial thermal conductance at CNT-substrate interfaces [12-19] and CNT-CNT junctions [20-24] are very low which can exacerbate the self-heating effects and can significantly degrade the TFT performance.

Studies of breakdown of a single CNT supported on SiO_2 substrate [12, 16] have demonstrated that the thermal boundary resistance (TBR) between CNTs and SiO_2 substrate limits the heat dissipation. The TBR is dependent on the CNT-substrate van der Waals (vdW) interactions, CNT diameter, and substrate roughness [16, 17]. The thermal energy exchange at the CNT-CNT interfaces (\sim CNT junctions) is even worse due to the weak interactions and small contact area. The large TBR at CNT junctions can have dominant effect on the heat transport in CNT networks which is highly dependent on the CNT spacing and overlap [23]. Experimental analysis in Reference [21] showed that the TBR at CNT junction can decrease by nearly two orders of magnitude (from 10^8 to 10^6 K/W) as the contact area increases from a cross contact to an aligned contact. The bulk thermal conductivity of a 3D random network of CNTs [24] can be as low as $0.13 \sim 0.20$ W/mK due to the low TBR at CNT junctions, which is even smaller than the thermal conductivity of the amorphous polymers used for the thermal insulation. The high electrical and thermal resistances at CNT junctions have been considered as the key factors that can limit the performance and reliability of CN-TFTs because they can cause hot spots, inefficient heat removal or even breakdown of CNTs [25]. Therefore, it is of great interest and importance to explore the thermal transport mechanism at CNT junctions and CNT-substrate interfaces.

Molecular dynamic (MD) simulations have been used in previous studies to estimate the TBR at CNT junctions and CNT-substrate interfaces and to investigate the roles of different phonon modes. These studies are based on the heat pulse analysis [26-29], direct methods [23, 30, 31], or transient relaxation

methods [14, 17, 32]. Although, the calculated TBR values have large variations in these studies due to the different CNT structures, empirical potential models, and statistical methodologies, a general agreement can be observed about the role of phonon modes in interfacial thermal transport. The large interfacial resistance between CNTs can be attributed to the weak vdW interactions [23] and small contact area. At CNT junctions, CNTs are non-bonded, and atoms interact through weak van der Waals forces. The modes which has strong inter-tube coupling such as bending, waving, and radial breathing are low frequency modes while the high frequency modes such as in-plane distortions and transverse modes has weak inter-tube coupling. [20, 26] The low frequency phonons are dominant heat carriers across CNT-SiO₂ interface as the transmission of high-frequency phonons (above a few tens of THz) is highly suppressed [22, 24]. Most of the previous studies were performed on isolated CNT junctions or CNT-substrate interfaces. In many applications such as CN-TFTs, the CNT network is supported on an oxide substrate [16, 25]. A close observation of these networks [16, 25] reveal that many CNTs may not be directly touching substrate, but partially or fully supported by other CNTs which can lead to the structures similar to shown in Fig. 1(b) or Fig. 1(c). Such structures can lead to the localized hot spots in the CNT networks and can pose severe reliability issues to the TFTs. Gupta *et al.* [33] analyzed the effects of TBRs at CNT interfaces on electrical breakdown of CN-TFTs using a coupled electro-thermal model. Their study also estimated the TBRs at CNT interfaces in CN-TFTs using the experimentally measured temperature distribution and power dissipation in TFTs. The phonon transport at these CNT junctions significantly affect TBR, temperature rise and hence CN-TFT performance and reliability. However, the phonon transport across CNT junction structures supported on a SiO₂ substrate has not been explored. Atomistic simulations of the thermal transport across such CNT structures can provide insights into possible modifications of molecular structure at the interface to enhance the phonon spectra matching and phonon mode coupling leading to better heat removal from the CN-TFTs [20].

In this study, we use molecular dynamics (MD) simulations to investigate the heat dissipation and phonon interactions at CNT junctions supported on SiO₂ substrate. We obtain the equilibrium

structures of the single CNT and CNT junctions supported on an oxide substrate (see Fig. 1), and demonstrate that at similar power densities the temperature in hanging CNTs (~ supported by only other CNTs) can be hundreds of degree higher compared to the CNTs well-contacted with the substrate leading to early breakdown. We investigate the decay of thermal energy in different frequency ranges using the spectral temperature. The high frequency phonons in CNTs (> 40 THz) do not have counterpart in SiO_2 substrate. However, they still have similar relaxation time as phonons in intermediate frequency range (5-40 THz), which suggests very fast intra-tube energy transfer in a CNT from high frequency band to intermediate frequency bands. We find that the low frequency phonon band (0-5 THz) of top CNT in a SiO_2 supported CNT junction have two-stage energy relaxation. The first stage with fast relaxation shows efficient coupling of low frequency phonons in CNT-oxide system. The second stage with very slow relaxation is consequence of blocking of the direct transport of high frequency phonons of top CNT to the oxide substrate by bottom CNT-

2 NUMERICAL METHODOLOGY

Molecular dynamics (MD) simulation is a promising method to study the interfacial thermal transport as different atomic configurations can be easily considered and phonon-phonon scattering events at interface including anharmonic effects can be inherently treated in a natural way [34, 35]. In this paper, we perform MD simulations on three configurations of CNT junctions (see Fig. 1) in order to develop an understanding of heat dissipation and phonon interactions in CNT networks supported on SiO_2 substrate. System I consists of a single CNT directly supported on the SiO_2 substrate, while the CNTs in System II and III are placed on one and two perpendicular CNTs, respectively. System II represents a typical crossed CNT junction in the CNT network of a CN-TFT, while system III represents CNTs in a high density network which is only supported by other CNTs and which do not make direct contact with the substrate. The substrate is periodic in x (length) and z (width) directions; it has 24,052 atoms and its dimensions are $285.0 \text{ \AA} \times 23.7 \text{ \AA} \times 59.6 \text{ \AA}$. We have checked the length effect by increasing the length of top CNT to 400 \AA and performing the thermal relaxation simulations (Section 3.1) for System I. No

obvious difference is observed in the estimated relaxation time. The distance between the two bottom CNTs in System III is half of the substrate length in x-direction which ensures a symmetric configuration on two sides from the center of substrate. The CNTs in the simulations have a chirality of (6, 0) and diameter of 4.7 Å. We use Lammmps package [36] for the molecular dynamics simulations. To describe C-C interactions in CNTs, we use the adaptive intermolecular reactive empirical bond order potential (AIREBO) [37]. For the amorphous SiO₂, we use the Munetoh parameterization [38] of the Tersoff potential to describe the Si-Si, O-O, and Si-O interactions. The vdW interactions between the CNT atoms at the interface are modeled by Lennard-Jones potential, $V_{ij}(r) = 4\epsilon_{ij} \left[\left(\frac{\sigma_{ij}}{r} \right)^{12} - \left(\frac{\sigma_{ij}}{r} \right)^6 \right]$. The present study employs the L-J parameterization used by Zhong and Lukes [23], with $\epsilon_{C-C} = 4.41 \text{ meV}$ and $\sigma_{C-C} = 0.228 \text{ nm}$. The vdW between the C-Si and C-O are also modeled using a L-J potential with the parameters from the universal force field (UFF) model by Rappe et al [39]. The parameters are $\epsilon_{C-Si} = 8.909 \text{ meV}$, $\epsilon_{C-O} = 3.442 \text{ meV}$, $\sigma_{C-Si} = 0.3326 \text{ nm}$, and $\sigma_{C-O} = 0.3001 \text{ nm}$ similar to parameters used in Reference [17, 18].

In the MD simulations, the atoms in the bottom layer of substrate are fixed to anchor the substrate. A time step of 0.25 fs is used for all simulations. In order to obtain the equilibrium structures, we first perform an energy minimization on the CNTs and amorphous SiO₂ system and then we equilibrate the system using NPT at 1 bar and 375 K for 1 ns. We applied a very small force (0.001 eV/Å on each atom) on the top CNT during the first 0.25 ns simulation in NPT to prevent the CNT to fly away from the system, and afterward the force is removed. Following the NPT equilibration, the volume of simulation box is determined, and the equilibration is continued using NVT at 375 K for 1 ns. The structures after equilibration are shown in Fig. 1. The deformation in CNTs due to the interaction with substrate is observed to be very small and its cross-section remains in circular shape after the equilibration, which is expected for small-diameter CNTs ($d < 21 \text{ Å}$) [16]. The single CNT in System I is completely supported by the substrate and remains straight after the equilibration like an isolated CNT. The top CNT in System II has a curvature near the region

supported by the bottom CNT. The minimum distance between the top CNT and SiO₂ substrate in System II is shown in Fig. 2. The curvature region spans 91 Å, which is about 20 times of the CNT diameter. As the spacing between the bottom CNTs supporting top CNT decreases, the top CNT get fully detached from the substrate as in System III and only has a slight bending toward the substrate at the ends.

3 RESULTS AND DISCUSSIONS

In order to elucidate the thermal transport at supported CNT junctions, we present the thermal analysis using two methods. The first one is the direct method of classical MD simulations where we examine the temperature distribution in CNT junctions and substrate by heating the top CNT (Section 3.1). In the second method, we study the transient energy relaxation in system (Section 3.2) by MD simulations and investigate the spectral energy decay using the spectral energy density (SED) approach. [14, 32]

3.1 Thermal Transport at CNT junction under High Power Density

In the direct MD method, we apply heating power in the range of 5 nW to 26.5 nW on the top CNT by rescaling the velocities of atoms. The maximum value 26.5 nW is selected following the experimental results [25] of the breakdown power of CNTs at high temperatures. A thermostat is applied to a 5Å thick region above the fixed layer of SiO₂ substrate to control its temperature at 375 K. The simulations are performed on the three configurations prepared by the equilibration (Fig. 1). Each case is simulated for 15 ns (25 ns for system III) to obtain a steady state, and then the data are sampled for 5 ns

During the sampling period, we calculate the temperature within 67 slabs along the CNT by

$$\frac{3}{2}nk_{\text{B}}T = \frac{1}{2}\sum_i^n m_i v_i^2 \quad (1)$$

where n is the number of atoms per slabs, and m_i and v_i are the mass and velocity of each atom. k_{B} is the Boltzmann's constant. Since the CNTs in the present simulations are relatively short and have very large thermal conductivity in the length direction, the temperature variations along the top CNTs are very

small. The top CNT in System I is in complete contact with the substrate and in system II is also primarily supported by the substrate; consequently small temperature variations ($< 3\text{K}$) has been observed. The top CNT in System III is supported by two bottom CNTs with a small contact. The section of top CNT between the supports can be treated as suspended CNT, and the contact with the bottom CNTs acts as heat sinks. The temperature distribution along the top CNT in System III at heating power of 26.5 nW is shown in Fig. 3; the variations are within 10 K , but larger than that in the other two Systems. The two minima in temperature are at coordinates of around -75 \AA and 75 \AA (Fig. 3), where the bottom CNTs are located. So the input power to top CNT is first transferred to two bottom CNTs through the small contact area at CNT junctions, and then conducted to the substrate through the bottom CNTs.

The temperature variation in top CNT at different heating power is shown in Fig. 4. The temperature rise for the fully supported (\sim System I) or partially supported CNT on SiO_2 (\sim System II) is not large, even at a high power density. However, the temperature increases rapidly when the top CNT is only supported by bottom CNTs and do not make any direct contact with the substrate (\sim System III). The contact area between the small diameter tubes is very small, and the inefficient heat conduction between CNTs can lead to this overheating in the top CNT at high power density. In our simulations, the temperature of top CNT increases beyond 834 K at the heating power of 26.5 nW which suggests that the breakdown temperature (873 K) [15, 25] will be easily reached in such CNTs even though the other CNTs in the network will be at much lower temperatures ($\sim 400\text{ K}$).

As shown in Fig. 2, the CNT contact area with the substrate in System II is reduced by 32% compared to System I but its temperature rise is only about 10 K (see Fig. 4) larger than that in System I. So it is of high interest to find how the heat is conducted to the substrate in System II. As shown in Fig. 5 (a), there are two heat conduction paths: (i) in the first path heat is directly conducted from top CNT to the substrate and the important thermal conductance is $g_{\text{CNT-sub}}$ (see System I), and (ii) in the second path heat is conducted first to bottom CNT and then to SiO_2 substrate; the important thermal conductance are $G_{\text{CNT-CNT}}$ and $g_{\text{CNT-sub}}$ (see System III). Due to the 1-D structure of CNT,

thermal conductance between CNT and substrate is defined as the rate of heat transfer per unit length (W/mK). Thermal conductance at CNT junction is not normalized with contact area and has unit of W/K. We can further assume interfacial thermal conductance through these two paths in System II equals to corresponding values in System I and III, respectively. Based on the thermal resistor circuit shown in Fig. 5 (a), the overall conductance from top CNT to SiO₂ substrate for each system can be obtained.

$$G_I = g_{\text{CNT-sub}} \cdot L \quad (2)$$

$$G_{II} = g_{\text{CNT-sub}} L_{\text{contact}} + \left(\frac{1}{G_{\text{CNT-CNT}}} + \frac{1}{g_{\text{CNT-sub}} \cdot L_B} \right)^{-1} \quad (3)$$

$$G_{III} = \left(\frac{1}{2G_{\text{CNT-CNT}}} + \frac{1}{2g_{\text{CNT-sub}} \cdot L_B} \right)^{-1} \quad (4)$$

Using the temperature response at different heating power (Fig. 4), thermal conductance $g_{\text{CNT-sub}}$ and $G_{\text{CNT-CNT}}$ can be determined. Thermal conductance $g_{\text{CNT-sub}}$ is estimated as 0.014 W/mK. Reference [17] gave an expression to estimate thermal conductance between CNT and SiO₂ substrate for the CNT diameter in the range of 0.81~1.63 nm and temperature in the range of 200~600 K. However, CNT diameter considered in our study is only 0.47 nm which is much smaller than the lower limit in Ref. [17]. If we extrapolate beyond the diameter range studied in Ref. [17], we estimate thermal conductance of 0.029 W/mK at 375K. The thermal conductance of CNT junction is 0.042 nW/K which is approximately twice of the value (~0.02 nW/K for CNTs with diameter of 0.5 nm) determined by atomistic Green's Function Calculations in Ref. [22]. Using thermal conductance $g_{\text{CNT-sub}}$ and $G_{\text{CNT-CNT}}$, the rate of heat transfer via two different paths in System II can be determined, as shown in Fig. 5 (b). It can be observed that heat is mainly conducted through the direct contact with the substrate, and less than 10% of the power is dissipated through the CNT-CNT junction. Since the CNTs have a high thermal conductivity, the heat generated in the buckled section of the top CNT can be first efficiently conducted along the tube to the sections supported by the SiO₂ substrate and then get dissipated to the substrate. Even if the contact length with the substrate is reduced by 32% in System II, the heat can still be effectively dissipated

through the reduced contact length (~ 18 nm) with a relatively small temperature rise. This agrees well with the previous measurements which suggest that relatively short contact lengths (10-30 nm) to a typical solid should be sufficient to transfer heat efficiently.[12]

We then calculate the overall thermal conductance at each interface in System III. Thermal conductance at CNT-CNT interfaces is about 0.084 nW/K which is half of the thermal conductance (0.172 nW/K) between bottom CNT and SiO₂ substrate. This indicates enhancing heat transfer at CNT junction will yield the largest gain. Besides, a low CNT junction density can also help to maintain a good contact between CNT and SiO₂ and avoid the fully suspended CNT structures as in System III; such CNTs should be removed from the CNT network in order to avoid hot spots.

3.2 Spectral Analysis of Heat Dissipation at CNT Junction

In order to investigate the role of phonon interactions in the interfacial thermal transport, we use the transient relaxation method and SED approach to obtain the transient decay of spectral temperature. In the simulations, we set an initial temperature difference ΔT between the top CNT and bottom CNTs/SiO₂ substrate. We set the bottom CNTs and SiO₂ substrate at 375 K and the top CNT at 600 K. This is achieved by first equilibrating the top CNT 600 K for 100 ps in the three configurations previously prepared by equilibration. The temperature of the bottom CNTs and SiO₂ substrate is kept at 375 K. The temperature is controlled by the velocity rescaling thermostat. Then, the thermostat is switched off, and the system is allowed to relax for 0.25 ns and 0.5 ns for System I and System III, respectively. The relaxation is simulated in a NVE ensemble. [17, 18] The temperature profile and the SED are averaged over every 10 time steps to reduce the random fluctuations of MD simulations.

We analyze the phonon energy distribution in the top CNT by calculating the SED. The SED is obtained by taking the Fourier transform of velocities of C atoms with respect to the frequency ω and wave vector k [32].

$$\theta(\omega, k) = \frac{m}{2} \sum_j^p \sum_\alpha^3 \left| \frac{1}{N} \sum_{n=0}^{N-1} \exp(ik_z z) \int v_{j,\alpha}(n, t) \exp(-i\omega t) dt \right|^2 \quad (5)$$

where p is the atoms in each unit cell, and N is the total number of unit cells in z direction. j, n , and α are the indices for p, N , and co-ordinate axes, respectively. The dispersion relations can be obtained by plotting the contour of the SED with respect to ω and k_z , as shown in Fig. 6(a). The wave vector is defined as $k_z = 2\pi n/a_z N$ where a_z is the lattice constant in z direction. The frequency dependence of the phonon energy distribution can be obtained by analyzing the spectrum of velocity which is determined by taking the Fourier transform of atom velocities with respect to frequency ω [32].

$$g(\omega) = \frac{1}{3N_a} \sum_j^{N_a} \sum_\alpha^3 \left| \int v_{j,\alpha}(t) \exp(-i\omega t) dt \right|^2 \quad (6)$$

where N_a is the total number of atoms. The normalized spectrum energy of C, O and Si atoms in System III are shown in Fig. 6(b). The spectral energy of C, Si, and O is normalized to the maximum value of spectral energy of C atoms in the top CNT. By assuming the energy is evenly distributed among all the phonon modes for CNTs at equilibrium, the equilibrium spectrum energy, g^{eq} , can be written as :

$$g^{\text{eq}}(\omega) = \rho(\omega) k_B T^{\text{eq}} \quad (7)$$

where $\rho(\omega)$ is the phonon density of states and T^{eq} is the equilibrium kinetic temperature. We further assume that $\rho(\omega)$ does not change during the transient relaxation, and introduce the spectral temperature $T_{\text{sp}}(\omega, t)$ [32]. The transient spectrum energy can be written as:

$$g^{\text{neq}}(\omega) = \rho(\omega) k_B T_{\text{sp}}(\omega, t) \quad (8)$$

In the calculation of transient spectrum energy, the short time Fourier transform is used. The velocities are sampled every 5 fs, which corresponds to the sampling rate of 200 THz. Then the entire time series are divided into blocks of 5 ps length and shift of 0.5 ps. Finally, we can determine the spectral temperature of each frequency band by

$$T_{sp}(t) = \frac{T^{eq}}{\omega_1 - \omega_2} \int_{\omega_1}^{\omega_2} \frac{g^{neq}(\omega)}{g^{eq}(\omega)} d\omega \quad (9)$$

In order to develop an understanding of the phonon coupling at the interfaces, we divide the entire frequency range into four bands, as shown in Fig. 6(b). Band 1 is the low frequency region below 5 THz which is most important for the energy transfer across interfaces. Band 2 and 3 corresponds to the frequency range of 5-12 THz and 12-40 THz. The overlap between the frequency spectrum of CNTs and SiO₂ exists in all the first three bands. Band 4 spans from 40 THz to 55 THz which has no overlap between frequency spectrum of CNTs and SiO₂. The SED $\theta(\omega, \mathbf{k})$ and the frequency dependence of the spectral energy $g(\omega)$ of the CNT in system I are similar to system III.

The transient decay of spectral temperature $T_{sp}(t)$ and its difference to the substrate temperature $\Delta T_{sp}(t)$ are shown in Fig. 7 (a) and (b) for system I and in Fig. 7 (c) and (d) for system III. We obtain the relaxation time constant, τ , of the spectral energy of each band by fitting the spectral temperature with an exponential function, i.e., $\Delta T_{sp}(t) = \Delta T_0 \exp(t/\tau)$. The relaxation time of the overall temperature of the top CNT in System I is 119 ps (Fig. 7 (b)). The spectral energy of band 1 decays fast with a relaxation time of 70 ps, while the spectral energies of the other three bands decays slowly with relaxation times (~115-121 ps) close to the overall temperature (Fig. 7 (b)). The fast relaxation of the low frequency spectral temperature indicates an efficient energy transfer across the interface, which confirms the importance of the low frequency phonons in the interfacial heat transfer.[18, 19] As shown in Fig. 6(b), there is no overlap in phonon spectrum of CNT and SiO₂ in band 4. It can be observed that ΔT_{sp} of the band 4 (not overlapping with SiO₂) also decays at nearly the same rate as the overall temperature. The phonons in band 4 of CNT have to dissipate energy to its own bands 1-3 (below 40 THz and overlapping with SiO₂) to transfer energy to SiO₂ substrate. This intra-tube energy transfer must be much faster than the interfacial energy transfer.[14] The similarity between the energy relaxation of bands 2, 3 and 4 may also indicates that the energy in band 4 primarily dissipate

to band 2 and 3 (Fig. 7(b)).

Compared to System I, System III has a much larger relaxation time (~ 1372 ps) for the overall temperature decay of the top CNT (Figs. 7 (c) and 7 (d)). The spectral temperature in band 2 to 4 decays similar to the overall temperature. However, the energy in band 1 has a two-stage decay characteristic, and cannot be described by a single relaxation time. So we fit the $\Delta T_{sp}(t)$ to the sum of two exponential functions: $\Delta T_{sp}^1(t) = \Delta T_{0,a} \exp(t/\tau_{1,a}) + \Delta T_{0,b} \exp(t/\tau_{1,b})$. The first stage is very fast with a relaxation time, $\tau_{1,a}$, of 47 ps, but the second stage is much slower ($\tau_{1,b} = 2132$ ps). In System III, the top CNT is supported only by bottom CNTs and have a small contact area and weak vdW interactions at the interface. The tube-tube energy transfer is mainly achieved by the low frequency phonons.[20, 22] As shown in Reference [22] using the atomic Green's function calculation, the phonon transmission above 10 THz is strongly suppressed, and this frequency threshold becomes even smaller for small diameter CNTs. For the CNT of chirality (6, 0) in this study, the phonon transmission has diminished to nearly zero for frequency above 8 THz.[22] In this stage the energy carried by low frequency phonons, which are excited during heating process, is transferred to the lower CNTs/ substrate rapidly due to the efficient coupling between the low frequency modes. The second stage ($\tau_{1,b} = 2132$ ps) may corresponds to the phase when the energy in high frequency bands (2 to 4) is first transferred to band 1 before getting transferred to lower CNT and the substrate. As shown in Fig. 7 (d), the time constant of spectral temperature relaxation is smallest for the highest frequency band but largest for the second stage of the low frequency band ($\tau_4 < \tau_3 < \tau_2 < \tau_{1b}$). This is because bottom CNTs block the energy transfer through the direct coupling of high frequency phonons and the energy from high frequency band need to be first transferred to the lower frequency band. The energy can get accumulated in these high frequency modes. As dominant energy content is in the high frequency bands, the slower relaxation of energy in high frequency bands (~ 2 to 4) to low frequency band (~ 1) as reflected in high $\tau_{1,b}$ and absence of direct coupling of high frequency phonons may become bottleneck for energy exchange at interface.

In system III, the bottom CNT works as a frequency filter which blocks the direct energy transfer via

the high frequency phonons from top CNT to substrate. Coupling of higher frequency phonons can help to enhance the heat transfer at CNT junctions, which may be achieved by nano-engineering the CNT-CNT interfaces through polymer wrapping, metal coating and linker molecules. [20, 40] Polymer molecules or smaller linker molecules can also be used as fillers to bridge the gap between top CNT and SiO₂. Besides, CNTs with larger diameter can have larger interfacial thermal conductance and contact area. [20, 33] But larger diameter can increase the buckling length of top CNTs, and thereby significantly reduce the contact area with substrate and deteriorate the heat dissipation around CNT junctions. [33]

CONCLUSIONS

In summary, the present study investigates the heat dissipation at CNT junctions supported on SiO₂ substrate using direct method and transient relaxation method of MD simulations. A CNT junction can reduce the contact of top CNT with the SiO₂ substrate by about 20 times of the CNT diameter, but the temperature of top CNT heated by high power does not increase rapidly until it becomes fully suspended. The relatively short contact length (~18 nm in present study) of CNT with substrate is sufficient for the heat removal at a high power density with an acceptable increase of temperature rise. However, CNTs fully suspended on other CNTs can reach to breakdown temperature at similar power density. In a CN-TFT with high density network such suspended CNTs will be prone to early breakdown. The role of phonons in the interfacial energy transfer in the supported CNT junctions is examined by analyzing the spectral temperature decay. The importance of the low frequency phonons in the interfacial thermal transport is confirmed by its fast relaxation. The bottom CNT in the supported CNT junctions blocks the direct transport of high frequency phonons of top CNT to the oxide substrate. The primary energy exchange in CNT-CNT-oxide junctions is through low frequency phonons in the range of 0-10 THz. The energy carried by these low frequency phonons in the fully suspended CNTs decays in two stages. The second stage seems to correspond to intra-tube energy exchange from high frequency bands to low frequency bands in top CNT and then

to the bottom CNT and substrate.

NOMENCLATURE

A contact area

E energy

G thermal boundary conductance

L length

N number of unit cells

T temperature

V potential energy

g spectral energy

j index for atoms in a unit cell

k index for unit cells

k_B Boltzmann constant

m atomic mass

n number of atoms

p number of atoms in a unit cell

t time

v velocity

Greek symbols

α index for dimensions

ε depth of potential well in L-J potential

θ spectral energy density

ρ phonon density of states

σ distance parameter in L-J potential

τ relaxation time constant

ω angular frequency

Subscripts

I system I

II system II

III system III

C carbon

Si silicon

O oxygen

Superscripts

eq equilibrium

neq non-equilibrium

sp spectral

ACKNOWLEDGEMENT

This work has been partly supported by the National Science Foundation Grant CBET-1236416 and CCF-1319935. We acknowledge technical discussion with Man Prakash Gupta (Georgia Institute of Technology) and Prof. Eric Pop (Stanford University).

REFERENCES

- [1] Baughman, R. H., Zakhidov, A. A., and de Heer, W. A., 2002, "Carbon nanotubes - the route toward applications," *Science*, 297(5582), pp. 787-792.
- [2] Reuss, R. H., Chalamala, B. R., Moussessian, A., Kane, M. G., Kumar, A., Zhang, D. C., Rogers, J. A., Hatalis, M., Temple, D., Moddel, G., Eliasson, B. J., Estes, M. J., Kunze, J., Handy, E. S., Harmon, E. S., Salzman, D. B., Woodall, J. M., Alam, M. A., Murthy, J. Y., Jacobsen, S. C., Olivier, M., Markus,

- D., Campbell, P. M., and Snow, E., 2005, "Macroelectronics: Perspectives on technology and applications," *P IEEE*, 93(7), pp. 1239-1256.
- [3] Cao, Q., and Rogers, J. A., 2009, "Ultrathin Films of Single-Walled Carbon Nanotubes for Electronics and Sensors: A Review of Fundamental and Applied Aspects," *Adv Mater*, 21(1), pp. 29-53.
- [4] Novak, J. P., Snow, E. S., Houser, E. J., Park, D., Stepnowski, J. L., and McGill, R. A., 2003, "Nerve agent detection using networks of single-walled carbon nanotubes," *Appl Phys Lett*, 83(19), pp. 4026-4028.
- [5] Snow, E. S., Novak, J. P., Lay, M. D., Houser, E. H., Perkins, F. K., and Campbell, P. M., 2004, "Carbon nanotube networks: Nanomaterial for macroelectronic applications," *J Vac Sci Technol B*, 22(4), pp. 1990-1994.
- [6] Kim, S., Kim, S., Park, J., Ju, S., and Mohammadi, S., 2010, "Fully Transparent Pixel Circuits Driven by Random Network Carbon Nanotube Transistor Circuitry," *Acs Nano*, 4(6), pp. 2994-2998.
- [7] Kim, S., Ju, S., Back, J. H., Xuan, Y., Ye, P. D., Shim, M., Janes, D. B., and Mohammadi, S., 2009, "Fully Transparent Thin-Film Transistors Based on Aligned Carbon Nanotube Arrays and Indium Tin Oxide Electrodes," *Adv Mater*, 21(5), pp. 564-568.
- [8] Valletta, A., Moroni, A., Mariucci, L., Bonfiglietti, A., and Fortunato, G., 2006, "Self-heating effects in polycrystalline silicon thin film transistors," *Appl Phys Lett*, 89(9), p. 093509.
- [9] Kumar, S., Pimparkar, N., Murthy, J. Y., and Alam, M. A., 2011, "Self-consistent electrothermal analysis of nanotube network transistors," *J Appl Phys*, 109(1), p. 014315.
- [10] Pop, E., Mann, D., Wang, Q., Goodson, K., and Dai, H. J., 2006, "Thermal conductance of an individual single-wall carbon nanotube above room temperature," *Nano Lett*, 6(1), pp. 96-100.
- [11] Kim, P., Shi, L., Majumdar, A., and McEuen, P. L., 2001, "Thermal transport measurements of individual multiwalled nanotubes," *Phys Rev Lett*, 87(21), p. 215502.
- [12] Maune, H., Chiu, H. Y., and Bockrath, M., 2006, "Thermal resistance of the nanoscale constrictions between carbon nanotubes and solid substrates," *Appl Phys Lett*, 89(1), p. 013109.
- [13] Tsai, C. L., Liao, A., Pop, E., and Shim, M., 2011, "Electrical power dissipation in semiconducting carbon nanotubes on single crystal quartz and amorphous SiO₂," *Appl Phys Lett*, 99(5), p. 053120.
- [14] Ong, Z. Y., and Pop, E., 2010, "Frequency and polarization dependence of thermal coupling between carbon nanotubes and SiO₂," *J Appl Phys*, 108(10), p. 103502.
- [15] Pop, E., Mann, D. A., Goodson, K. E., and Dai, H. J., 2007, "Electrical and thermal transport in metallic single-wall carbon nanotubes on insulating substrates," *J Appl Phys*, 101(9), p. 093710.
- [16] Liao, A., Alizadegan, R., Ong, Z. Y., Dutta, S., Xiong, F., Hsia, K. J., and Pop, E., 2010, "Thermal dissipation and variability in electrical breakdown of carbon nanotube devices," *Phys Rev B*, 82(20), p. 205406.
- [17] Ong, Z. Y., and Pop, E., 2010, "Molecular dynamics simulation of thermal boundary conductance between carbon nanotubes and SiO₂," *Phys Rev B*, 81(15), p. 155408.
- [18] Ong, Z. Y., Pop, E., and Shiomi, J., 2011, "Reduction of phonon lifetimes and thermal conductivity of a carbon nanotube on amorphous silica," *Phys Rev B*, 84(16), p. 165418.
- [19] Grujicic, M., Cao, G., and Gersten, B., 2004, "Atomic-scale computations of the lattice contribution to thermal conductivity of single-walled carbon nanotubes," *Mat Sci Eng B-Solid*, 107(2), pp. 204-216.
- [20] Xu, Z. P., and Buehler, M. J., 2009, "Nanoengineering Heat Transfer Performance at Carbon Nanotube Interfaces," *Acs Nano*, 3(9), pp. 2767-2775.
- [21] Yang, J. K., Waltermire, S., Chen, Y. F., Zinn, A. A., Xu, T. T., and Li, D. Y., 2010, "Contact thermal resistance between individual multiwall carbon nanotubes," *Appl Phys Lett*, 96(2), p. 023109.
- [22] Chalopin, Y., Volz, S., and Mingo, N., 2009, "Upper bound to the thermal conductivity of carbon nanotube pellets," *J Appl Phys*, 105(8), p. 084301.
- [23] Zhong, H. L., and Lukes, J. R., 2006, "Interfacial thermal resistance between carbon nanotubes: Molecular dynamics simulations and analytical thermal modeling," *Phys Rev B*, 74(12), p. 125403.

- [24] Prasher, R. S., Hu, X. J., Chalopin, Y., Mingo, N., Lofgreen, K., Volz, S., Cleri, F., and Koblinski, P., 2009, "Turning Carbon Nanotubes from Exceptional Heat Conductors into Insulators," *Phys Rev Lett*, 102(10), p. 105901.
- [25] Estrada, D., and Pop, E., 2011, "Imaging dissipation and hot spots in carbon nanotube network transistors," *Appl Phys Lett*, 98(7), p. 073102.
- [26] Chen, L., and Kumar, S., 2011, "Thermal transport in double-wall carbon nanotubes using heat pulse," *J Appl Phys*, 110(7), p. 074305.
- [27] Kumar, S., and Murthy, J. Y., 2009, "Interfacial thermal transport between nanotubes," *J Appl Phys*, 106(8), p. 084302.
- [28] Osman, M. A., and Srivastava, D., 2005, "Molecular dynamics simulation of heat pulse propagation in single-wall carbon nanotubes," *Phys Rev B*, 72(12), p. 125413.
- [29] Shiomi, J., and Maruyama, S., 2006, "Non-Fourier heat conduction in a single-walled carbon nanotube: Classical molecular dynamics simulations," *Phys Rev B*, 73(20), p. 205420.
- [30] Diao, J., Srivastava, D., and Menon, M., 2008, "Molecular dynamics simulations of carbon nanotube/silicon interfacial thermal conductance," *J Chem Phys*, 128(16), p. 164708.
- [31] Thomas, J. A., Iutzi, R. M., and McGaughey, A. J. H., 2010, "Thermal conductivity and phonon transport in empty and water-filled carbon nanotubes," *Phys Rev B*, 81(4), p. 045413.
- [32] Carlborg, C. F., Shiomi, J., and Maruyama, S., 2008, "Thermal boundary resistance between single-walled carbon nanotubes and surrounding matrices," *Phys Rev B*, 78(20), p. 205406.
- [33] Gupta, M. P., Chen, L., Estrada, D., Behnam, A., Pop, E., and Kumar, S., 2012, "Impact of thermal boundary conductances on power dissipation and electrical breakdown of carbon nanotube network transistors," *J Appl Phys*, 112(12), p. 124506.
- [34] Cahill, D. G., Ford, W. K., Goodson, K. E., Mahan, G. D., Majumdar, A., Maris, H. J., Merlin, R., and Phillpot, S. R., 2003, "Nanoscale thermal transport," *J Appl Phys*, 93(2), pp. 793-818.
- [35] Maruyama, S., 2002, "A molecular dynamics simulation of heat conduction in finite length SWNTs," *Physica B*, 323(1-4), pp. 193-195.
- [36] Plimpton, S., 1995, "Fast Parallel Algorithms for Short-Range Molecular-Dynamics," *J Comput Phys*, 117(1), pp. 1-19.
- [37] Stuart, S. J., Tutein, A. B., and Harrison, J. A., 2000, "A reactive potential for hydrocarbons with intermolecular interactions," *J Chem Phys*, 112(14), pp. 6472-6486.
- [38] Munetoh, S., Motooka, T., Moriguchi, K., and Shintani, A., 2007, "Interatomic potential for Si-O systems using Tersoff parameterization," *Comp Mater Sci*, 39(2), pp. 334-339.
- [39] Rappe, A. K., Casewit, C. J., Colwell, K. S., Goddard, W. A., and Skiff, W. M., 1992, "Uff, a Full Periodic-Table Force-Field for Molecular Mechanics and Molecular-Dynamics Simulations," *J Am Chem Soc*, 114(25), pp. 10024-10035.
- [40] Varshney, V., Patnaik, S. S., Roy, A. K., and Farmer, B. L., 2010, "Modeling of Thermal Conductance at Transverse CNT-CNT Interfaces," *J Phys Chem C*, 114(39), pp. 16223-16228.

Figure Captions

Figure 1. Configurations of (a) System I, (b) System II, and (c) System III. These Systems are equilibrated at 375K.

Figure 2. Minimum distance between top CNT and SiO₂ substrate in System II (see Fig. 1 (b)). Here, $x=0$ corresponds to the mid-point of the bottom CNT.

Figure 3. Temperature distribution along the top CNT in System III at heating power of 26.5 nW.

Figure. 4. Temperature variations of top CNT in the three Systems shown in Fig. 1 as a function of heating power.

Figure 5. (a) Equivalent thermal resistor circuit of Systems I, II and III. (b) Rate of heat transfer via CNT-SiO₂ direct contact and CNT-CNT junction in System II. L and L_B are the lengths of top and bottom CNTs, respectively. L_{contact} is the length of top CNT directly contacted with SiO₂ in System II.

Figure. 6. (a) Phonon dispersion relations of top CNT in system III at T=375 K. k^* is wave vector normalized with respect to $2\pi/a_z$. (b) Normalized phonon spectral energy of system III at different frequencies at T=375 K. The spectral energy of C (in top and bottom CNTs), Si, and O is normalized to the maximum value of spectral energy of C atoms in top CNT. The frequency ranges of four phonon bands (1-4) are shown.

Figure. 7. Top CNT total temperature, substrate temperature, and spectral temperature (T_{sp}) of four frequency bands (see Fig. 6 (b)) of top CNT in (a) System I and (c) System III. The transient decay of difference between top CNT total temperature (or spectral temperature of phonon bands) and substrate temperature (ΔT) for (b) System I and (d) System III. The unit of time constant is picosecond.

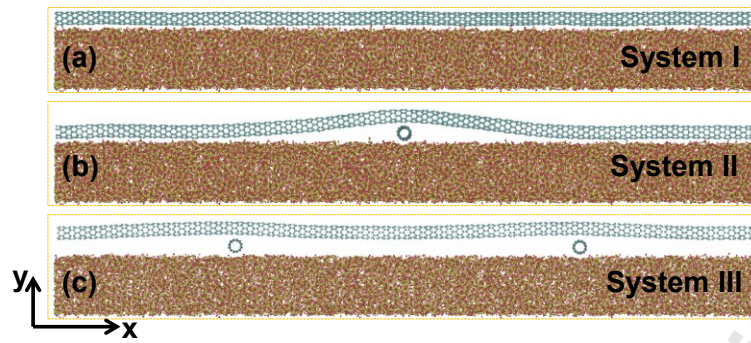


Figure 1. Configurations of (a) System I, (b) System II, and (c) System III. These Systems are equilibrated at 375K.

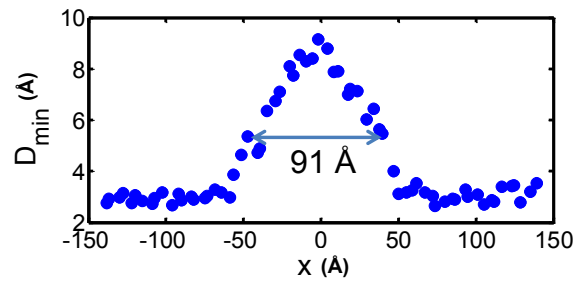


Figure 2. Minimum distance between top CNT and SiO₂ substrate in System II (see Fig. 1 (b)). Here, $x=0$ corresponds to the mid-point of the bottom CNT.

Accepted Manuscript Not Copyedited

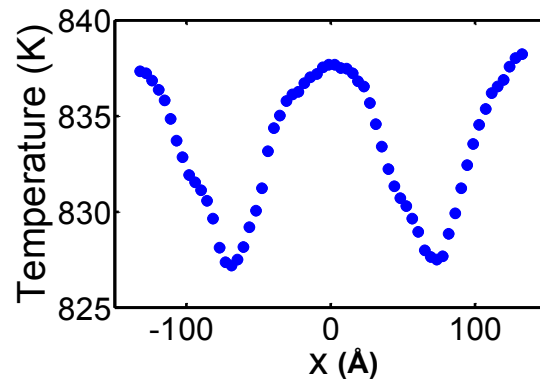


Figure 3. Temperature distribution along the top CNT in System III at heating power of 26.5 nW.

Accepted Manuscript Not Certified

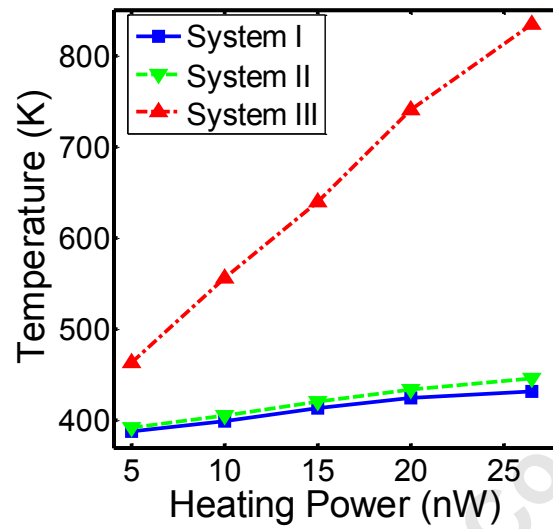


Figure. 4. Temperature variations of top CNT in the three Systems shown in Fig. 1 as a function of heating power.

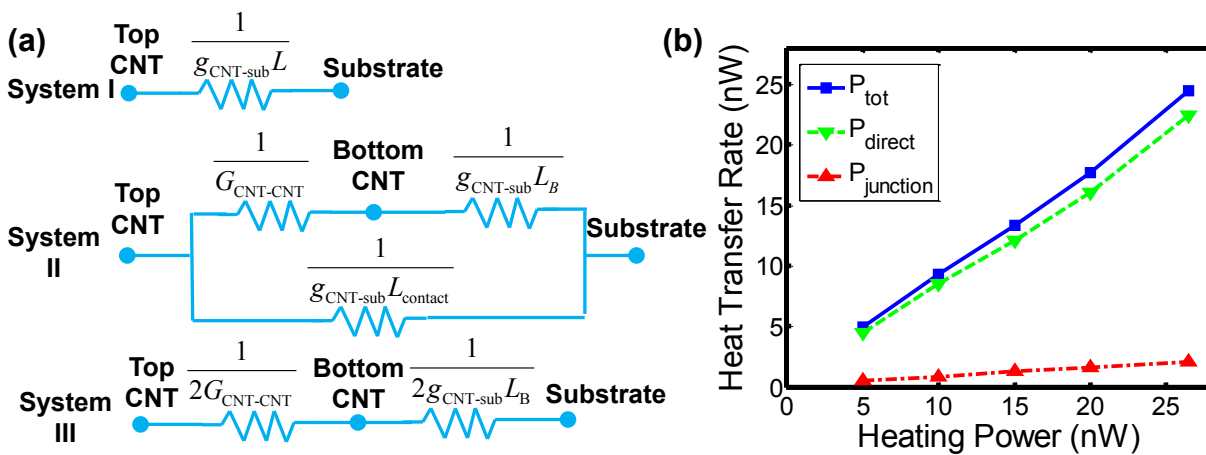


Figure 5. (a) Equivalent thermal resistor circuit of Systems I, II and III. (b) Rate of heat transfer via CNT-SiO₂ direct contact and CNT-CNT junction in System II. L and L_B are the lengths of top and bottom CNTs, respectively. L_{contact} is the length of top CNT directly contacted with SiO₂ in System II.

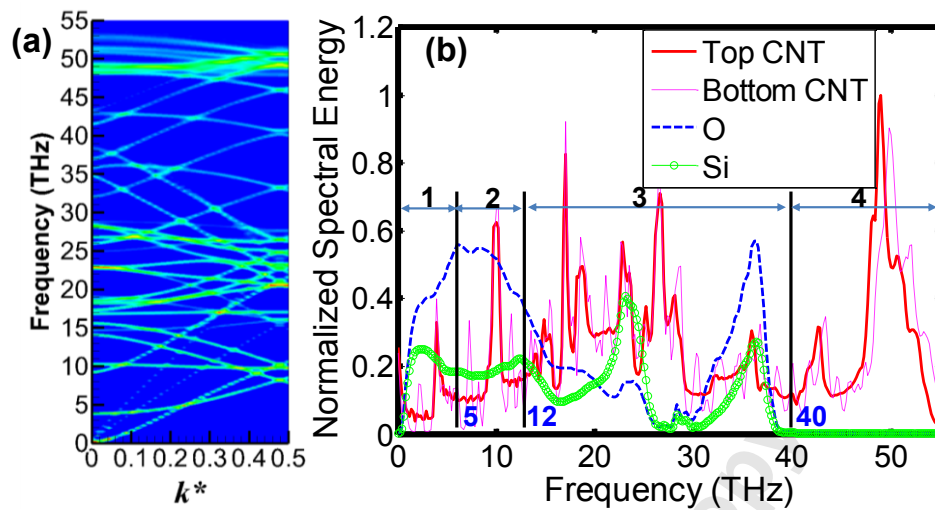


Figure. 6. (a) Phonon dispersion relations of top CNT in system III at $T=375$ K. k^* is wave vector normalized with respect to $2\pi/a_z$. (b) Normalized phonon spectral energy of system III at different frequencies at $T=375$ K. The spectral energy of C (in top and bottom CNTs), Si, and O is normalized to the maximum value of spectral energy of C atoms in top CNT. The frequency ranges of four phonon bands (1-4) are shown.

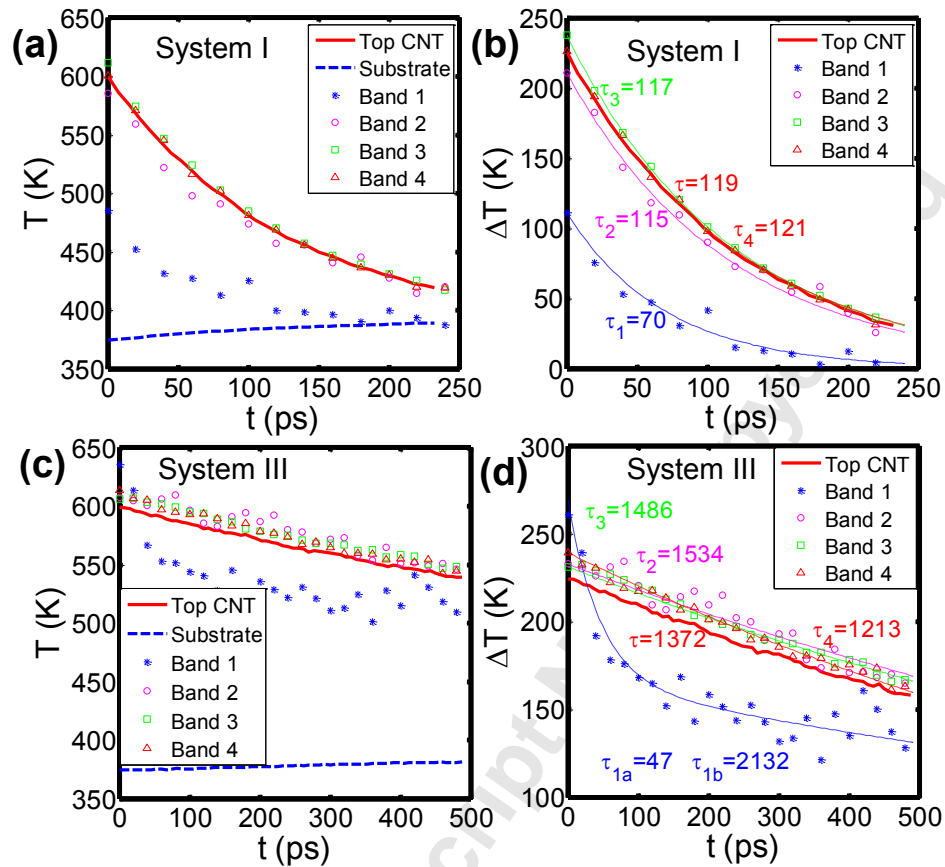


Figure. 7. Top CNT total temperature, substrate temperature, and spectral temperature (T_{sp}) of four frequency bands (see Fig. 6 (b)) of top CNT in (a) System I and (c) System III. The transient decay of difference between top CNT total temperature (or spectral temperature of phonon bands) and substrate temperature (ΔT) for (b) System I and (d) System III. The unit of time constant is picosecond.